FULL LENGTH ARTICLE

Narciclasine induces colon carcinoma cell apoptosis by inhibiting the IL-17A/Act1/TRAF6/NF-κB signaling pathway

Huiming Deng [a,b,1], Qiang Liu [c,1], Siman Yu [d,1], Lifan Zhong [b,e], Lianfang Gan [b,e], Huiquan Gu [c], Qianru Wang [b,e], Ruxin Cheng [b,e], Yong Liu [a], Li Liu [a], Ling Huang [b,e,f,**], Ronghua Xu [a,*]

[a] *Department of Gastrointestinal Surgery, Huazhong University of Science and Technology Union Shenzhen Hospital, Shenzhen, Guangdong 518000, China*
[b] *Research Center for Drug Safety Evaluation of Hainan Province, Haikou, Hainan 571199, China*
[c] *Department of Pharmacology, Hainan Medical University, Haikou, Hainan 571199, China*
[d] *Department of Pathology, Guangzhou Panyu Central Hospital, Guangzhou, Guangdong 511400, China*
[e] *Hainan Province Key Laboratory for Drug Preclinical Study of Pharmacology and Toxicology Research, Hainan Medical University, Haikou, Hainan 571199, China*
[f] *Hainan Center for Drug and Medical Device Evaluation and Service, Hainan Medical Products Administration, Haikou, Hainan 570216, China*

Abstract IL-17 A is a promoter of colorectal cancer initiation and progression. Narciclasine is a polyhydroxy alkaloid compound isolated from *Narcissus* plants, which has potent anti-inflammatory and antitumor actions. The effects of narciclasine on colorectal tumors were evaluated, with a focus on IL-17 A. Narciclasine reduced the growth of HCT-116 and SW-480 colon cancer cells *in vitro* and *in vivo* in murine xenografts. The results of flow cytometry on JC-1 and Annexin V/PI revealed that narciclasine significantly reduced the mitochondrial membrane potential and induced apoptosis, findings confirmed by western blotting results of reduced Bcl-2 and enhanced Bax expression, as well as accumulation of cleaved Caspase-3, Caspase-8, Caspase-9, and cytoplasmic Cytochrome-c. After narciclasine incubation, IL-17 A, Act1, and TRAF6

* Corresponding author. Department of Gastrointestinal Surgery, Huazhong University of Science and Technology Union Shenzhen Hospital, No. 89 Taoyuan Road, Shenzhen, Guangdong 518000, China.
** Corresponding author. Research Center for Drug Safety Evaluation of Hainan Province, No. 3 Xueyuan Road, Haikou, Hainan 571199, China; Hainan Center For Drug and Medical Device Evaluation and Service, Hainan Medical Products Administration, No. 53 Nanhai Road, Haikou, Hainan 570216, China.
E-mail addresses: puer6@163.com (L. Huang), hyfyweichang@163.com (R. Xu).
Peer review under responsibility of Chongqing Medical University.
[1] These authors contributed equally to this work.

were down-regulated, while p-P65 (Ser536) accumulated in the cytoplasm, a finding confirmed by laser scanning confocal microscopy. IL17A substitution could partly reverse these narciclasine effects while they were elevated by IL17A silencing. Moreover, IL-17 A, Act1, and TRAF6 were significantly expressed to greater extents in human colorectal cancer compared to normal adjacent tissue specimens and were closely linked with a poor prognosis. This study provided evidence that narciclasine may be a useful therapeutic drug for colorectal cancer treatment through its actions in down-regulating the L-17A/Act1/TRAF6/NF-κB anti-apoptotic signaling pathway.

Introduction

Colorectal cancer (CC) has affected about 1.9 million people globally and is responsible for about 0.9 million premature deaths in 2020 and has ranked as the second most deadly cancer.[1] Therefore, finding efficient and low-toxic colon cancer chemotherapy drugs and effective therapeutic targets will be vital to improve the survival rates and quality of life of CC patients.

Interleukin-17 A (IL-17 A) has potent pro-inflammatory properties and is secreted from *T* helper 17 cells (Th17) and plays a fundamental role in the genesis of various disease states, being recently implicated as a novel therapeutic target for cancer. Increasing research focuses on IL-17 because it has been shown to promote tumor resistance to inhibition of vascular endothelial growth factor (VEGF) through nuclear factor-κB (NF-κB) and extracellular-related kinase (ERK) signaling in multiple tumor models.[2] It also blocks the response of tumors to anti-programmed cell death protein 1 immunotherapy in CC cells.[3]

Signal transduction through IL-17 A starts with the formation of heterodimers after IL-17 A binds to the IL-17 A receptor (IL-17RA), which then recruits nuclear factor-κB activator 1 (Act1) to form an IL-17RA-Act1 complex. The complex stimulates the formation of tumor necrosis factor receptor-associated factor-6 (TRAF6) and IκB kinases (IKKs), which relieves the inhibition of nuclear factor kappa B (IκB) on NF-κB, leading to nuclear translocation of NF-κB and related gene transcriptions.[4–6] High serum concentrations of IL-17 A are associated with a worse prognosis for patients undergoing anti-angiogenesis therapy[7] and IL-17 A has been reported to be a good biomarker for the diagnosis and eventual prognosis of CC patients.[8] IL-17 A also promotes the development of colitis-associated cancer and the cycle progression of CC cells as well as metastasis and invasion of CC cells through NF-kB-mediated matrix metalloproteinase up-regulation.[9] In a murine CC model, it was demonstrated that IL-17 A increased the expression of PD-L1 by actions on the p65/NRF1/miR-15 b-5p axis. It also increased resistance to anti-PD-1 treatment, while inhibiting the IL-17 A-stimulated improvement in the effectiveness of treatment with anti-PD-1.[3]

Narciclasine (Ncs) is a polyhydroxy alkaloid compound isolated from *Narcissus* plants[10] that has potent antitumor and anti-inflammatory actions.[11] Previous studies have shown that it can induce apoptosis that is autophagy-dependent in breast cancer cells that are triple-negative,[12] prolong survival in a murine brain cancer model,[13] and reduce by 50% *de novo* protein synthesis in endothelial cells.[14] In addition, apoptosis induced by Ncs in human MCF-7 breast and PC-3 prostate cancer cells was highly selective, with a 250 times lower toxicity than in human fibroblasts.[15]

Here, the effects of Ncs on CC cells and its underlying mechanisms were investigated, with a focus on the IL-17A/Act1/TRAF6 axis associated with apoptosis.

Materials and methods

Reagents and chemicals

Ncs with a purity ≥99.9% were purchased from Chengdu Herbpurify CO., LTD, and recombinant human interleukin-17 A (Rh-IL-17 A) from GenScript (China). Mitochondrial membrane potential (MMP) assay kits with JC-1, cell cycle and apoptosis analysis kits, DAPI, H&E stains, and an MTT cell proliferation and cytotoxicity assay kit were purchased from Beyotime Biotechnology.

Patient specimens

A total of 191 CC tissue samples and 183 adjacent non-cancerous tissue specimens were obtained from patients enrolled in the study, namely, 91 paired CC and adjacent tissues from Sun Yat-sen Memorial Hospital, 6 paired CC and adjacent tissues from Guangzhou Panyu Central Hospital, and 94 CC tissue samples and 86 noncancerous tissues contained in tissue microarray chips from Shanghai Outdo Biotech (HColA180Su21, China). No patients received preoperative chemotherapy or radiotherapy and all sample diagnoses were confirmed by two experienced pathologists. Each enrolled patient provided informed consent and tissue specimen collection was approved by the Huazhong University of Science and Technology Union Shenzhen Hospital Scientific Research Ethics Committee.

Cell culture and cell transfection

CC SW-480, HCT-116, HT-29, LS174T, and LOVO cell lines were all cultured at 37 °C in a sterile incubator with 5% CO_2 added to the atmosphere. The growth medium was RPMI-

1640 supplemented with fetal bovine serum (10%), penicillin (100 U/mL), and streptomycin (100 mg/mL).

IL-17 A scrambled small interfering RNA (siRNA) was made by OBio (China), with the following sequences: sense: 5′-CCCAAAGGUCCUCAGAUUTT-3′; antisense: 5′-AAUCU-GAGGACCUUUUGGGTT-3′. The si-IL-17 A was then transfected with Lipofectamine 2000 reagent for 24 h following the manufacturer's protocol.

Viability of cells and colony formation

The cell viability and colony formation assays were conducted as previously described.[16] Essentially, cells were plated at a density of 5×10^3 cells per well. After exposure to Ncs at concentrations of 0.125, 0.25, 0.5, 1.0, 2.0, and 4.0 µmol/L for 24 h, 10 µL of a solution of 5 mg/mL MTT was added to wells, which were then incubated for a further 4 h. Next, the well medium was replaced with DMSO (120 µL) to dissolve the formazan dye which allowed the measurement of absorbance at 570 nm (SpectraMaxM4, MD Company, USA). This procedure permitted the determination of cell viability and the subsequent evaluation of IC_{50} values using GraphPad software. Both cell types at an initial density of 200 cells per well were exposed to increasing Ncs concentrations (vide supra). Cells were incubated for 14 days, with the medium being replaced every 48 h. Cell colonies were visualized after 0.1% crystal violet staining (Sigma—Aldrich, USA), images were captured using an IX73 microscope (Olympus, Japan), and subsequently, cells were counted using Image J software (NIH, USA).

Confocal microscopy observations

Each cell type was treated with Ncs (0.5 µM) for 24 h, thoroughly washed in PBS, and then fixed for 20 min in a solution of 4% paraformaldehyde. Subsequently, cells were exposed to 0.1% TritonX-100 for 20 min to disrupt them before they were blocked using 10% FBS. Next, cells were incubated with phospho—NF—κB65 (p-P-65, Ser563, Cell Signaling Technology, USA, #3033) rabbit primary antibody (1:600) overnight at 4 °C. DAPI (10 ng/mL) was used to stain cell nuclei and images were visualized and digitally captured using a confocal microscope (Olympus, Japan).

Molecular docking

The structure of Ncs was manufactured using JSME and then converted to 3D with minimized energy using MM2 force field. The crystal structure of IL-17 A (PDB code: 4HR9) was fetched from a RCSB protein data bank (http://www.rcsb.org/). After calculating Gasteiger charges, water molecules were deleted from the target protein by employing Autodocktools version 1.5.6 software, while nonpolar hydrogen was added. After being imported into Autodocktools, atomic charges were added and the atomic types specified, and all flexible bonds were rotated by default as docking ligands. The best-scored result, visualized by Discovery Studio (2016), was output after the docking operation of Autodock Vina version 1.1.2. After modeling by the Swiss-model server, the proteins with the most similar structure to that of Act1, TRAF6, and IKKα/β

fetched from the Uniprot data bank (https://www.uniprot.org/) were selected. Next, structures were imported into the Schrodinger Program and the following procedures were used to obtain optimization of each structure and minimization of the energy for docking, including assignment of bond orders using the database CCD, addition to hydrogens, the creation of zero-order bonds to metal and disulfide bonds, termination of the cap, deletion of excess water, as well as generating het states using Epic.

Immunoprecipitation

RIPA buffer (P0013B, Beyotime Biotechnology, China) was used to lyse cells and the concentrations of proteins in samples were measured with a BCA kit (Beyotime Biotechnology). IP assays were conducted by closely following the instructions supplied with the assay kit (Invitrogen, USA). Briefly, 1 mg of extracted protein in 500 µL was incubated with 4 µg of specific antibodies (overnight at 4 °C) and immunoprecipitated using Dynabeads® M—280 tosylactivated magnetic beads (4 h at 4 °C). Next, beads were adsorbed onto a magnetic shelf and thoroughly washed 3 times. After centrifugation, SDS buffer (40 µL) was added, and the beads were heated to 95 °C for 10 min and then analyzed using western blotting.

Western blotting

Harvested cells were lysed in RIPA buffer and the concentration of protein in each sample was measured using the bicinchoninic acid assay (P0010S, Beyotime Biotechnology). Nuclear and cytoplasmic isolates were separated (P0027, Beyotime Biotechnology) and the protein bands were separated using 8%—14% SDS-PAGE before being transferred to PVDF membranes, which were blocked with 5% dry skim milk for 1 h at ambient room temperature (circa 18 °C-20 °C) and washed three times with TBST. Following the block, membranes were exposed to various primary antibodies, namely, IL-17 A (1:1,000, ab79056), NF-κB P65 (P65, 1:1,000, ab32536), Bax (1:1000, ab32503), Bcl-2 (1:1000, ab32124), Cytochrome c (1:1,000, ab13575), Caspase-3 (1:1000, ab32351), Caspase-8 (1:1,000, ab108333), Caspase-9 (1:1,000, ab202068), Ki-67 (1:1,000, ab92742), IκBα (1:1,000, ab32518), IKKα (1:1,000, ab178870), GAPDH (1:1,000, ab8245) (Abcam, USA), phospho-P65 (S536) (1:1,000, #3033), phospho-IKKα/β (S176/S180) (1:1000, #2697), phospho-IκBα (S32) (1:1,000, #2859), TRAF6 (1:1,000, #8028) (Cell Signaling Technology, USA), and Act1 (1:1,000, SC-100647) (Santa Cruz Biotechnology, USA). Next, they were exposed to the corresponding secondary antibodies at ambient room temperature (1:5,000, MultiSciences, Shanghai, China). Lastly, the target proteins were examined with enhanced chemiluminescence chemicals (P0018, Beyotime Biotechnology), and visualized and quantified using a ChemiDoc XRS system (BIO-RAD, USA). Full and uncropped western blots are presented in Additional File 1.

Transcriptome sequencing

RNA after isolation was purified following exposure to TRIzol reagent (Invitrogen, USA), and the purity and total

amount were determined using NanoDrop ND-1000. The RNA veracity was evaluated using a Bioanalyzer 2100 (Agilent, US), with a RIN number >7 confirmed using denaturing agarose gel electrophoresis. One microgram sample of Poly(A) RNA was purified on Dynabeads in 2 purification steps. Next, the sample was broken into fragments (94 °C, for 5−7 min) using a Magnesium RNA Fragmentation Module (NEB, USA). The cleaved fragments of RNA were reverse-transcribed by employing SuperScript™ II Reverse Transcriptase to create cDNA. The resultant cDNA was utilized to make U-labeled second-stranded DNAs with *E. coli* DNA polymerase I and RNase H (both sourced from NEB) and a solution of dUTP (Thermo Fisher). An A-base was attached to the end of strands to facilitate ligation to indexed adapters. After heat-labile UDG enzyme treatment of the U-labeled second-stranded DNAs, constructs were amplified using PCR with a first denaturation of 3 min at 95 °C; 8 cycles for 15 s each at 98 °C; annealing for 15 s at 60 °C; extension for 30 s at 72 °C; and a last extension for 5 min at 72 °C. Finally, 2×150 bp paired-end sequencing was carried out using Illumina Novaseq 6000.

Analyses of apoptosis and MMP

Both cell types were seeded onto well plates and exposed to Ncs (0.25, 0.5 μmol/L) for 24 h. After harvesting, following thorough washing in PBS solution, the cells were resuspended in a binding buffer (500 μL). Then, 5 μL of Annexin V-FITC and 10 μL of propidium iodide were added and the mixture was incubated for 10 min at 4 °C under light-free conditions. The extent of apoptosis was evaluated with an Accuri C6 flow cytometry cell analyzer. To measure the cell membrane potential both cell types were treated according to the above conditions, and after being washed with PBS, 1 mL of JC-1 was added and the solution was thoroughly mixed, before further incubation (20 min, 37 °C). After aspiration of the supernatant, cells were centrifuged and washed in pre-cooled JC-1 buffer before being resuspended in 1 mL of fresh buffer. Changes in cell membrane potentials were measured using a flow cytometry cell analyzer (Accuri C6, USA). For laser scanning confocal microscopy analysis, cells were first washed in PBS solution and then incubated in 1 mL of cell culture medium plus 1 mL of JC-1 staining solution (20 min, 37 °C). The supernatant was removed and washed twice in JC-1 buffer and membrane potentials were measured using an Olympus confocal microscope.

Xenograft assays

Procedures involving animals were performed in accordance with the Guidelines for the Humane Treatment of Laboratory Animals (Ministry of Science and Technology of the People's Republic of China, Policy No. 2006398). All experiments were approved by the Huazhong University of Science and Technology Union Shenzhen Hospital Scientific Research Ethics Committee. Twenty-four BALB/c nude mice (aged 4 weeks) were provided by Alac Laboratory Animal Co. Ltd (certificate number: 20170005037900). The mice were kept in sterile cages at 20 °C−25 °C and a humidity of 40%−70%, with *ad libitum* access to drinking water and standard laboratory chow. 5×10^6 cells in 100 μL of PBS were injected subcutaneously into the left flanks of each mouse's armpit. Tumors grew to approximately 50 mm^3 in volume and nude mice were randomly allocated into an Ncs group (5 mg/kg, Q.3 d, p. o., $n = 6$) or a normal saline group (5 mL, Q.3 d, p. o., $n = 6$). Every 3 days, the rate of tumor growth was monitored and their volumes were calculated using the following equation: V = (length of width)^2 × (length of length)/2 Mice were humanely killed after treatment for 21 days and tumors were excised and carefully weighed. Subsequently, the tumors were fixed in 4% formalin for immunohistochemistry analyses and H&E staining.

H&E staining

Tumor tissue, heart, liver, kidney, stomach, and intestinal specimens were set in blocks of paraffin, and sections of 4-μm thickness were produced, which were then stained with H&E (Sigma−Aldrich, USA) for histopathological assay. Images were captured on a light microscope (BX43, Olympus Co., Ltd., Japan).

Immunohistochemistry (IHC)

The IHC assays and IHC scores were performed using a previously described protocol.[16] High expression levels were defined as a sum of scores ≥ 4 points, while low expression levels were considered the sum of scores < 4 points.

Statistical analysis

All evaluations of data were made using either GraphPad Prism (version 8.0) or SPSS (version 21.0, Abbott Laboratories, USA). Data are presented as mean $\pm$ standard deviation (SD) when normally distributed. To look for potential differences between groups, *t*-tests or one-way ANOVA were employed, with a post hoc Bonferroni correction applied. A chi-squared test was used to analyze the clinical pathological characteristics of the data. Kaplan−Meier and log-rank methods were employed to evaluate survival analysis. A correlation analysis was conducted using a two-sided Pearson correlation. *P*-values < 0.05 were deemed statistically significant. $^{*}P < 0.05$, $^{**}P < 0.01$, $^{***}P < 0.001$; ns, no significance.

Results

Ncs inhibited the proliferation of cells but promoted apoptosis

As shown in Figure 1A, exposure of cells to Ncs for 24 h markedly decreased the viability of the CC cell lines HT-29, HCT-116, LS174T, SW-480, and LOVO in a concentration-dependent manner; the IC$_{50}$ values were 0.575 μM, 1314 μM, 0.567 μM, 1.074 μM, and 1.405 μM, respectively. Further analysis revealed that 0.5 μM and 1.0 μM Ncs incubation for 24 h reduced the clone colony formation of both HCT-116 and SW-480 cells (Fig. S1A).
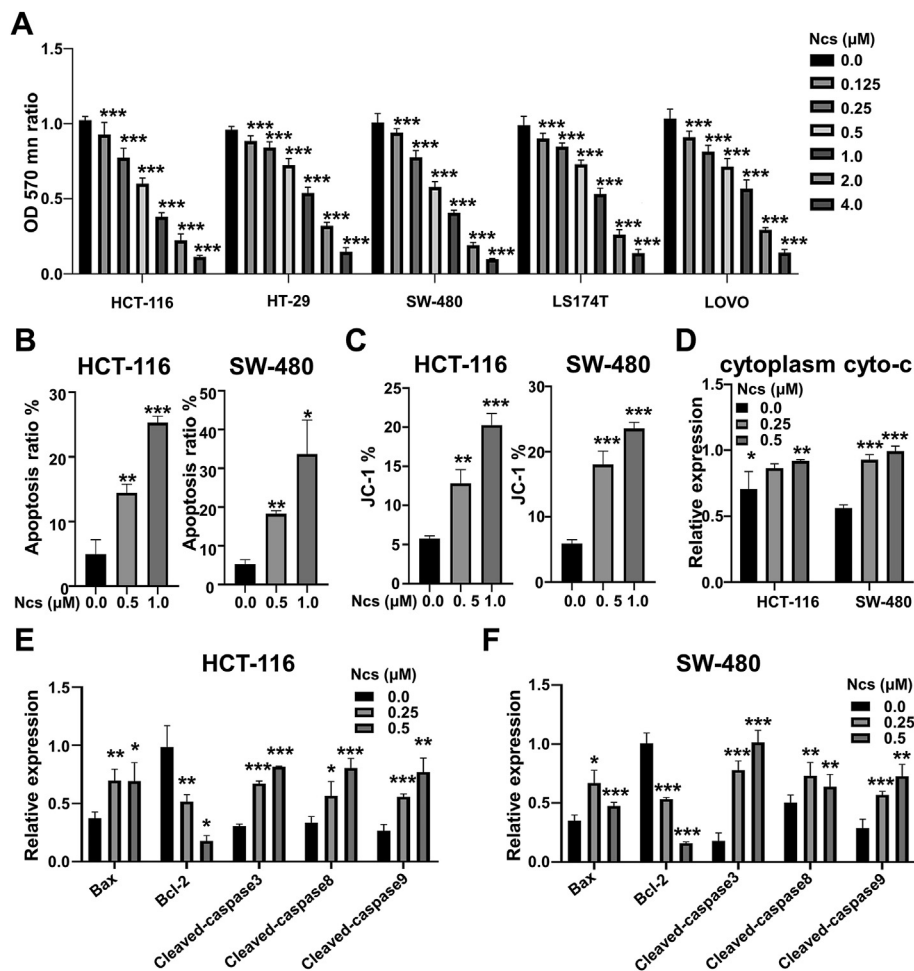
Figure 1 Ncs inhibited the growth of CC cells and promoted mitochondrial apoptosis *in vitro*. **(A)** CC cells were treated with Ncs for 24 h and their growth was measured using an MTT assay. **(B)** Cells were treated with Ncs and apoptotic cells were stained with PI/Annexin-V, followed by flow cytometry analysis. **(C)** Flow cytometry was employed for the measurement of MMPs in conjunction with a JC-1 assay. **(D)** Western Blot results of cytochrome-c levels in the cytoplasm of HCT-116 and SW-480 cells. **(E, F)** Western blot results of the levels of apoptosis-related proteins Bax, cleaved Caspase-3, Caspase-8, and Caspase-9, and Bcl-2 in HCT-116 (E) and SW-480 (F) cells exposed to Ncs for 24 h. Data are given as mean $\pm$ SD and are representative of 3 independent experiments. Statistical difference was analyzed using one-way ANOVA with a post hoc Bonferroni correction.

Next, we investigated whether Ncs was regulating apoptosis in CC cells. An Annexin V/Propidium Iodide apoptosis assay revealed that 0.25 μM and 0.5 μM Ncs treatment of cells induced apoptosis in a concentration-dependent manner (Fig. 1B; Fig. S1B), findings confirmed by JC-1 membrane potential analyses (Fig. 1C; Figs. S1C, D). Apoptosis induction by Ncs was further supported by the increased cytoplasmic Cytochrome-c levels and enhanced expression of Bax, cleaved Caspase-3, Caspase-8, and Caspase-9, as well as a lower expression of Bcl-2 in both cell types (Fig. 1D–F; Fig. S1E). Collectively, these results demonstrated that Ncs had a considerable anti-cancer effect in CC cells by promoting mitochondrial apoptosis.

Ncs inhibited the IL-17A/Act1/TRAF6/NF-κB signaling pathway to induce CC cell apoptosis

In order to clarify Ncs-mediated apoptosis in CC cells, mRNA was extracted from HCT-116 CC cells that had been treated with Ncs for 24 h and subjected to transcriptome analysis. Compared to the controls, KEGG pathway analysis revealed that IL-17 A and NF-κB signaling pathways were significantly different (Fig. 2A). Previous studies have shown that IL-17 A can up-regulate the NF-κB pathway[6] and Act1/TRAF6-mediated NF-κB activation in autoimmune and inflammatory diseases.[17] Based on these previous studies, we further explored whether the role of Ncs in promoting apoptosis was related to IL-17A/Act1/TRAF6/NF-κB signaling. In order to evaluate the interactions between Ncs and IL-17 A, an *in-silico* analysis was performed. The free energy of binding was −6.67 kcal/mol and Ncs formed hydrogen bonds with Gln94, Leu97 of the IL-17 A A chain, and Trp67 of the B chain. van der Waals forces were formed with Lle96, Glu95 of the A chain, and Val98, 117, 119, Lle96, and Pro63 of the B chain, in addition to π-alkylation (Pi ALK) bonds with Lle66 of the B chain (Fig. S2).

The expression of IL-17 A, Act1, TRAF6, and NF-κB pathway-related proteins was also investigated using western blotting. Ncs treatment significantly inhibited the
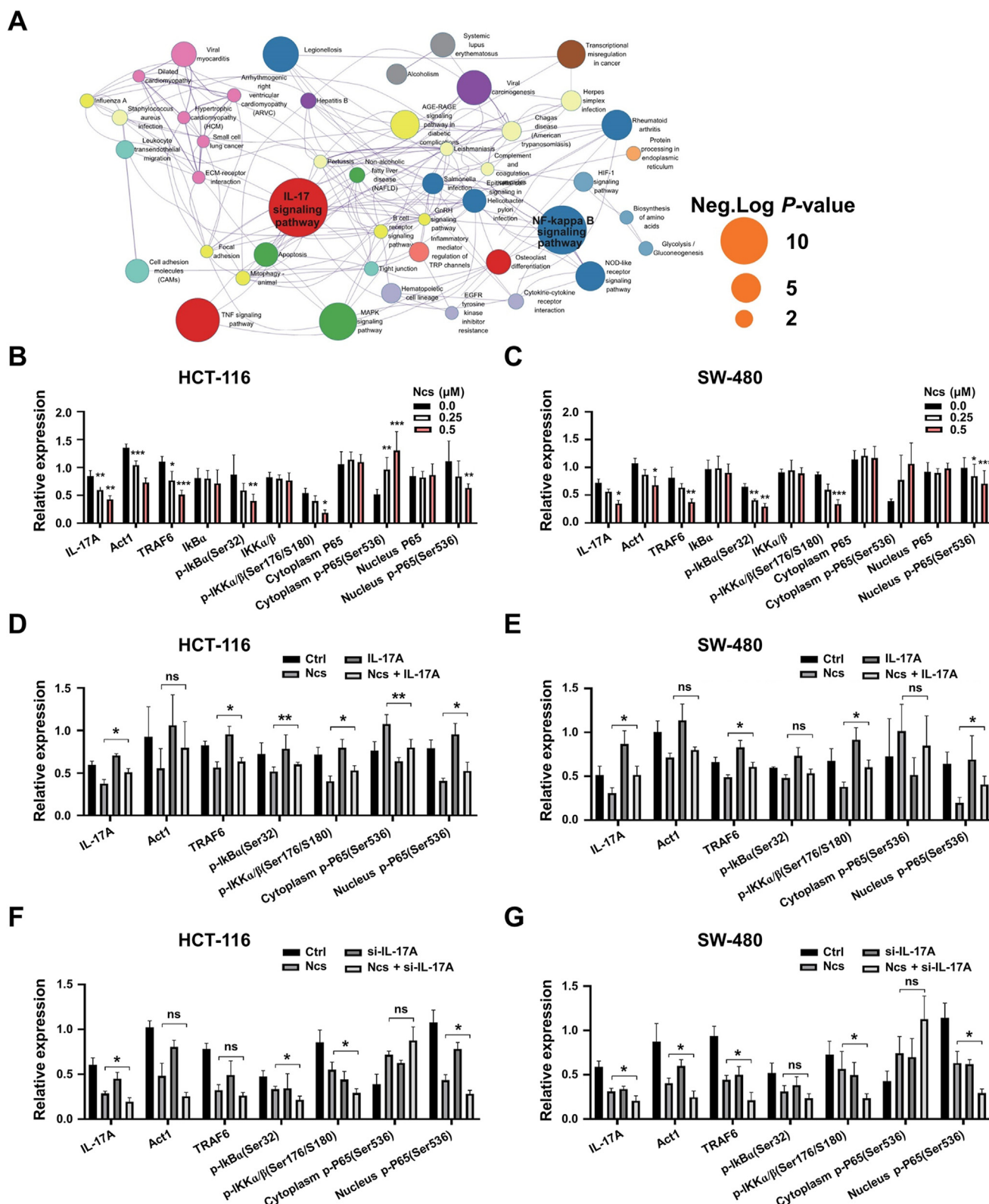
Figure 2   Ncs inhibits IL-17A/Act1/TRAF6/NF-κB signaling pathway *in vitro*. **(A)** CC HCT-116 cells were exposed to 0.5 μM Ncs for 24 h versus controls and a genome (KEGG) pathway enrichment was constructed by transcriptome sequencing. The sizes of the dots indicate negative $\log_{10}$ (*P*-value). Cells were exposed to Ncs for 24 h and the cell lysates were used to analyze the expression of IL-17 A, Act1, TRAF6, IκBα, IKKα/β, p-IκBα (Ser32), p-IKKα/β (Ser176/180), P65, and p-P65 (Ser536) in **(B)** HCT-116 cells and **(C)** SW-480 cells using western blotting. **(D)** HCT-116 and **(E)** SW-480 cells were exposed to 100 ng/mL Rh-IL-17 A or **(F, G)** si-IL-17 A in the absence and presence of Ncs (0.5 μM) for 24 h. Expression levels of IL-17 A, Act1, TRAF6, p-IκBα(Ser32), p-IKKα/β (Ser176/180), and p-P65 (Ser536) were detected by western blotting. Data are given as mean ± SD and are representative of 3 independent experiments. Statistical difference was analyzed using one-way ANOVA with a post hoc Bonferroni correction.
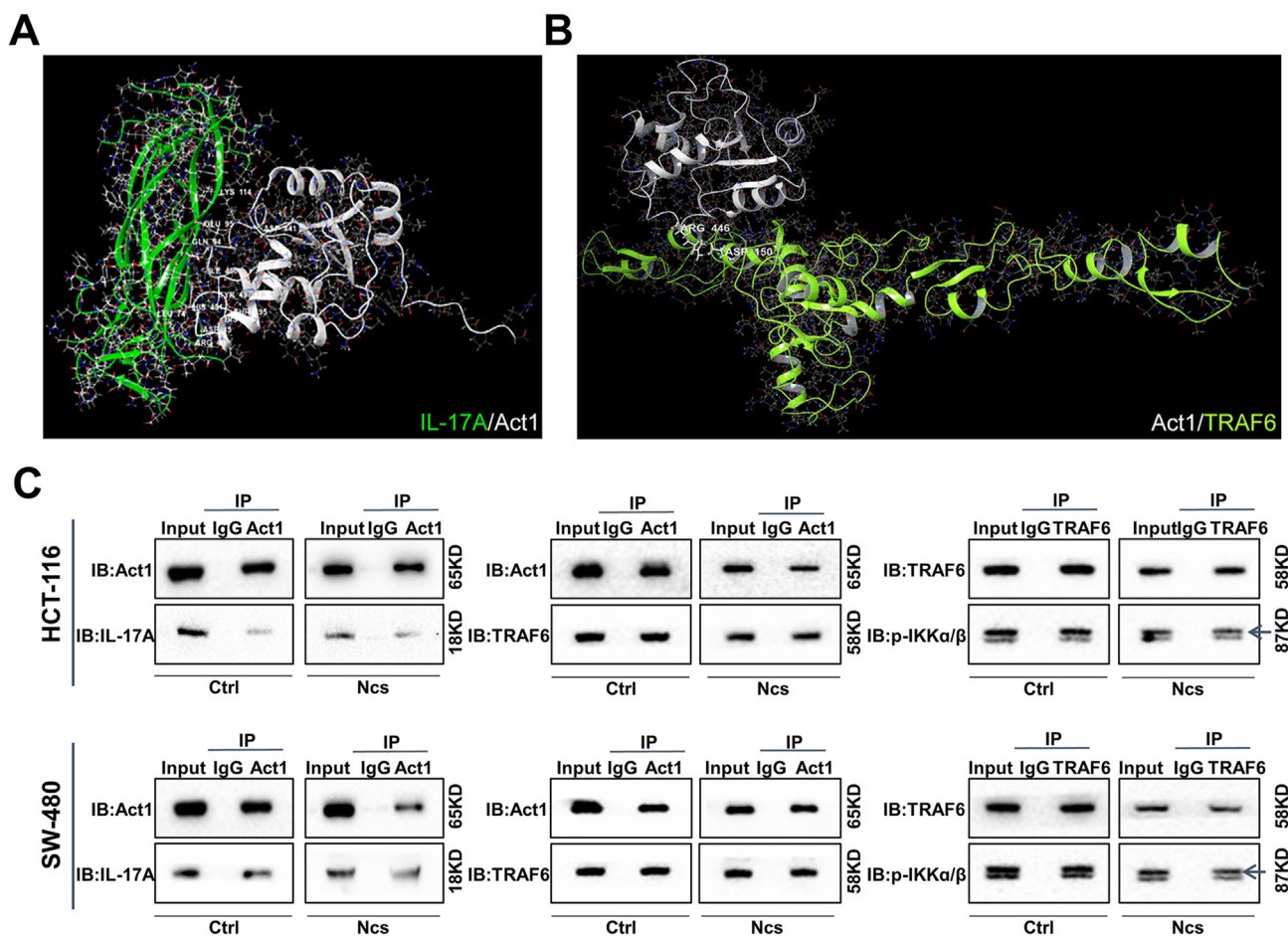
Figure 3 Molecular docking of IL-17 A and Act1, Act1 and TRAF6, as well as TRAF6 and p-IKKα/β (Ser176/180). **(A)** A three-dimensional diagram showing the binding conformation of IL-17 A (green) with Act1 (silvery white) and **(B)** of Act1 (silvery white) with TRAF6 (green). **(C)** Interactions between IL-17At and Act1, Act1 and TRAF6, TRAF6 and p-IKKα/β (Ser176/180) in the absence and presence of Ncs treatment were determined by co-immunoprecipitation assays.

expression of IL-17 A, Act1, and TRAF6, decreased the phosphorylation of IκBα (Ser32) and IKKα/β (Ser176/180), and reduced the nuclear translocation of p-P65 (Ser536). However, IκBα, IKKα/β, and P65 did not significantly change their locations between the inside and outside of the nucleus, but p-P65 (Ser536) was translocated to the cytoplasm (Fig. 2B, C; Fig. S3A), which was also observed using a confocal microscope (Fig. S3B). Of note, when 100 ng/mL of Rh-IL-17 A was supplemented to both cell types, the inhibitory actions of Ncs were mostly rescued, especially in HCT-116 cells, with increased nuclear p-P65 (Ser536) translocation (Fig. 2D, E; Fig. S3E). In contrast, combinatorial treatment of both cell types with si-IL-17 A and Ncs further reduced the expression of IL-17 A, Act1, TRAF6, p-IκBα (Ser32), and p-IKKα/β (Ser176/180). The treatment also enhanced the accumulation of p-P65 (Ser536) in the cytoplasm and reduced its nuclear translocation (Fig. 2F, G; Fig. S3E).

To strengthen these results, molecular docking analysis and immunoprecipitations were used to clarify whether IL-17 A and Act1, Act1 and TRAF6, TRAF6 and p-IKKα/β interacted and whether Ncs weakened the interaction between them. Molecular docking analysis indicated that IL-17 A and Act1, Act1 and TRAF6, TRAF6 and p-IKKα/β were closely integrated (Fig. 3A, B; Fig. S4 and Tables S1—3). The same results were found after immunoprecipitation assays, while the interactions between IL-17 A and Act1, Act1 and TRAF6, TRAF6 and p-IKKα/β were weakened in CC cells after Ncs treatment (Fig. 3C). These data suggest that L-17 A regulates NF-κB activity via Act1 and TRAF6, and that Ncs can inhibit IL-17A/Act1/TRAF6/NF-κB signaling pathway in CC cells.

In order to confirm associations with the IL-17A/Act1/TRAF6/NF-κB signaling pathway and related Ncs effects to apoptosis, cells were further analyzed. IL-17 A supplementation reduced the degree of apoptosis induced by Ncs and the decline in MMP, while Ncs synergistically enhanced si-IL-17 A-induced apoptosis and the decline in MMP (Fig. 4A, B). Rh-IL-17 A significantly restored cleaved Caspase-3, Caspase-8, and Caspase-9, and Cytochrome-c expression levels in CC cells that had been exposed to Ncs (Fig. 4C, D). Conversely, si-IL-17 A further elevated the degree of expression of Caspase-3, Caspase-8, and Caspase-9, and elevated cytoplasmic Cytochrome-c in Ncs-treated

HCT-116 and SW-480 cells (Fig. 4E, F). Taken together, these data indicate that the IL-17A/Act1/TRAF6/NF-κB axis is a vital signaling pathway for Ncs-induced mitochondrial apoptosis of CC cells.

The growth of CC cells was inhibited by Ncs *in vivo*

To evaluate *in vivo* actions of Ncs on CC cell growth, a murine xenograft model was established by inoculating human HCT-116 and SW-480 CC cells subcutaneously into nude mice. The growth rate of xenografts in Ncs-treated mice was significantly lower than that in the controls, while tumor size and tumor weights were markedly reduced in Ncs-treated mice (Fig. 5A–C). In addition, the H&E stain was employed to measure the amount of nuclear division. Immunohistochemical analysis of the expression density of Ki-67 was used to confirm the change in the proliferation status of CC cells. The numbers of mitotic proliferating cells and the expression density of Ki-67 in cells treated with Ncs were significantly lower than those in the controls (Fig. 5D).

Moreover, Ncs treatment produced no significant detectable pathological features on the heart, liver, and kidney, and only produced a relatively minor sub-inflammation of the stomach and intestine (Fig. 5E; Fig. S5A). The IHC results also showed that Ncs treatment could reduce the expression levels of IL-17 A, Act1, TRAF6, and p-P65 (Ser536) in xenograft tissues (Figs. S5B, C). These data indicated that Ncs exhibit anti-cancer effects on CC *in vivo* and that the IL-17A/Act1/TRAF6/NF-κB axis is a potential pathway for Ncs-mediated anti-CC effects.

IL-17 A, Act1, and TRAF6 were highly expressed in CC tissue and correlated with a poor prognosis for CC patients

Protein levels of IL-17 A, Act1, and TRAF6 were evaluated in 191 CC tissues and in 183 non-cancer tissues to explore whether the IL-17A/Act1/TRAF6 axis could be traced in human CC tissue specimens. As shown in Figure 6A and B, immunohistochemical analyses revealed that IL-17 A, Act1, and TRAF6 expression levels were up-regulated in CC specimens compared to non-cancerous specimens, whereas the positive rates of IL-17 A, Act1, and TRAF6 were significantly lower in non-cancer tissue (Fig. 6C), indicating that IL-17 A, Act1, and TRAF6 were up-regulated in CC. The level of IL-17 A in CC tissue was positively associated with Act1 and TRAF6 levels, and Act1 levels were positively correlated with TRAF6 expression in CC tissue (Fig. 6D). Kaplan–Meier analyses appeared to indicate that IL-17 A, Act1, and TRAF6 up-regulation was significantly associated with a shorter overall survival time in CC patients, but only Act1 reached statistical significance (Fig. 6E).

IL-17 A ($P = 0.03$) and TRAF6 ($P = 0.01$) expression levels were significantly correlated with poor tumor differentiation, as well as for Act1 ($P = 0.002$) with lymph node metastasis (Table 1 and Fig. 7A).

Discussion

In the previously published literature, IL-17 was reported to be a vital factor involved in the genesis of CC.[18] It is believed that T cells that produce IL-17 in pathological microenvironments contribute to the pathogenesis of ulcerative colitis and link chronic inflammation to CC-initiating cell development,[19,20] while this effect was prevented in a murine colitis-associated cancer model using IL-17 A deficient mice as the negative control.[21] Besides, the conclusions of another murine enterotoxigenic *Bacteroides fragilis*-driven CC model study stressed the importance of targeting IL-17 itself, rather than its cellular sources, since they found redundant innate and adaptive sources of IL-17 production which were responsible for CC tumorigenesis.[22] We demonstrated that there was an ectopic expression of IL-17 A in HCT-116 and SW-480 cells, which has also been reported for breast, lung, and CC cells[23–25] as well as been proposed to be implicated in epithelial and smooth muscle cell responses in benign prostate hyperplasia.[26] When IL-17 A was overexpressed in CT26 CC cells using gene transfer, in particular, membrane-bound IL-17 A enhanced their proliferation rate through up-regulated cell cycle progression.[27]

Apoptosis, also known as programmed cell death, is recognized as an important factor in inducing cell death during cancer treatment.[28] When cancer cells are affected by various stimuli, the MMP will increase and Cytochrome-c located in the mitochondrial membrane gap will be released into the cytoplasm where it will bind to apoptotic protease activating factor 1, which activates Caspase-9 and downstream Caspase-3, thereby triggering the Caspase cascade reaction and inducing apoptosis.[29,30] The regulation of Cytochrome-c release is mainly dependent on the Bcl-2 protein family. Bcl-2-asslciated X Protein (Bax) is transferred from the cytoplasm to the mitochondria after cells are stimulated by apoptotic signals, and the permeability of the mitochondrial membrane is destroyed leading to Cytochrome-c release.[31] On the other hand, Bcl-2, an anti-apoptotic protein, is located in mitochondria where it helps maintain the MMP and prevent the release of Cytochrome-c thus inhibiting apoptosis. Bcl-2 can form dimers with Bax, which block the anti-apoptotic effect of Bcl-2 when Bax is activated.[32] This study showed that Ncs reduced the proliferation of both HCT-116 and SW-480 CC cells and inhibited their xenograft growth. The xenograft experiments also revealed that Ncs had no toxic effects on the heart, liver, and kidneys of nude mice, which is in line with the findings of previous studies.[11,15] Flow cytometry and protein expression analyses also revealed that Ncs reduced the MMP as well as promoted Cytochrome-c secretion and the expression of Bax, in addition to inhibiting the expression of Bcl-2, thereby initiating the Caspase cascade reaction and apoptosis.

Further *in vitro* IL-17 A overexpression and silencing experiments revealed that anti-apoptotic IL-17A/Act1/TRAF6-mediated NF-kB transcription was inhibited by Ncs blocking the actions of IL-17 A. NF-kB expression has been
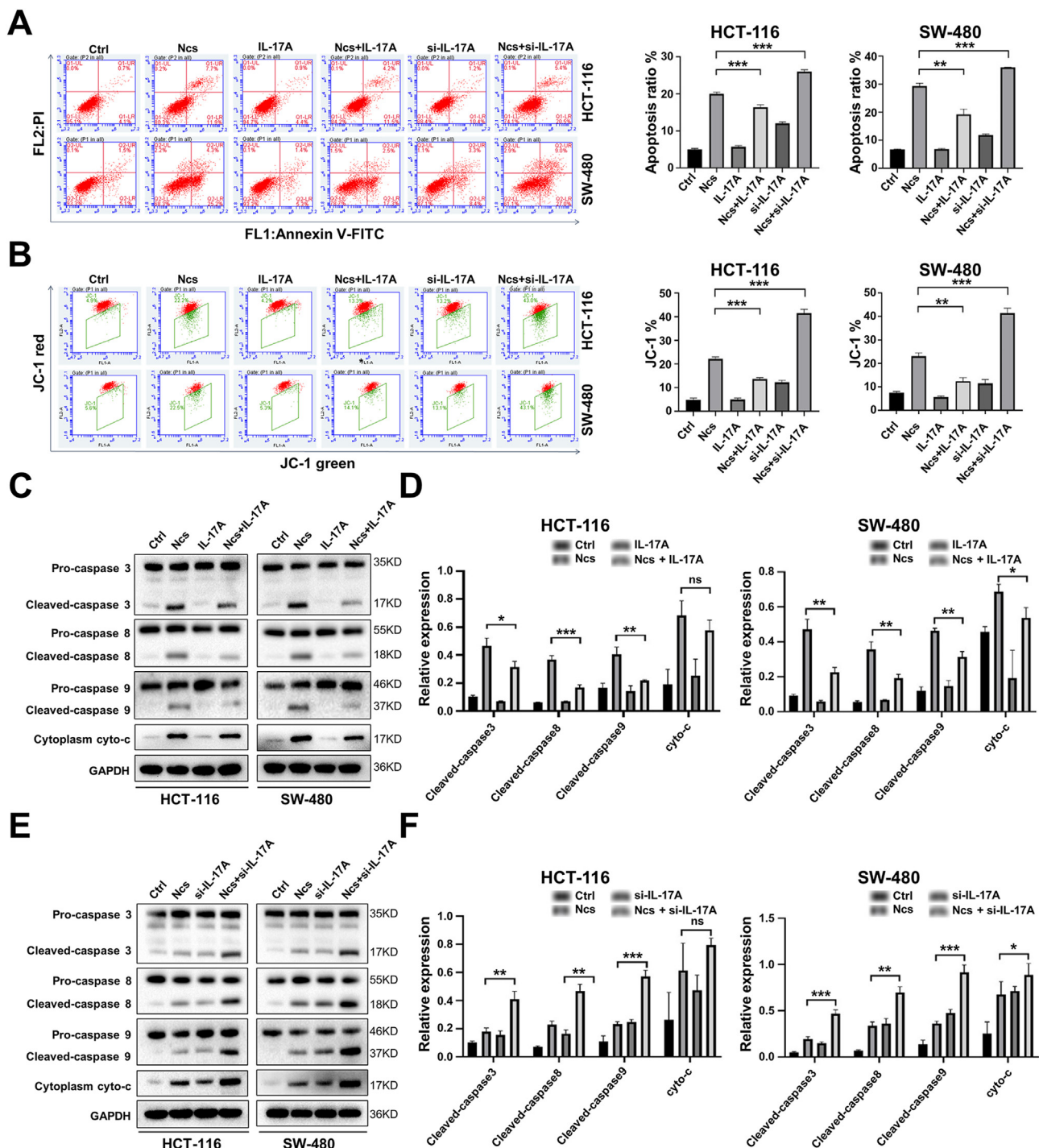
Figure 4 Ncs induces mitochondrial apoptosis of CC cells through an IL-17 A-regulated signaling pathway. CC HCT-116 and SW-480 cells were treated with si-IL-17 A or Rh-IL-17 A (100 ng/mL) in the presence and absence of Ncs (0.5 μM) for 24 h. **(A)** Apoptotic cells were stained with PI/Annexin-V and examined using flow cytometry. **(B)** MMP was measured by flow cytometry after staining with JC-1. Western blotting results of expression levels of apoptosis-related proteins **(C, D)** after IL-17 A (100 ng/mL) and **(E, F)** after silencing of IL-17 A. Data are given as mean ± SD and are representative of 3 independent experiments. Statistical difference was analyzed using one-way ANOVA with a post hoc Bonferroni correction.

shown to inhibit the apoptosis of CC cells.[33] The immuno-histochemistry analyses of human CC tissue samples revealed that IL-17 A, Act1, and TRAF6 also exhibited enhanced expression in CC compared to adjacent tissues in the present study. IL-17 A, Act1, and TRAF6 up-regulation

was associated with a shorter overall survival time for CC patients. Interestingly, the level of increased IL-17 A mRNA in colorectal adenomas, a hallmark for the progression toward cancer, was associated with the severity of dysplasia in a previous study.[34] TRAF6 has previously been shown to
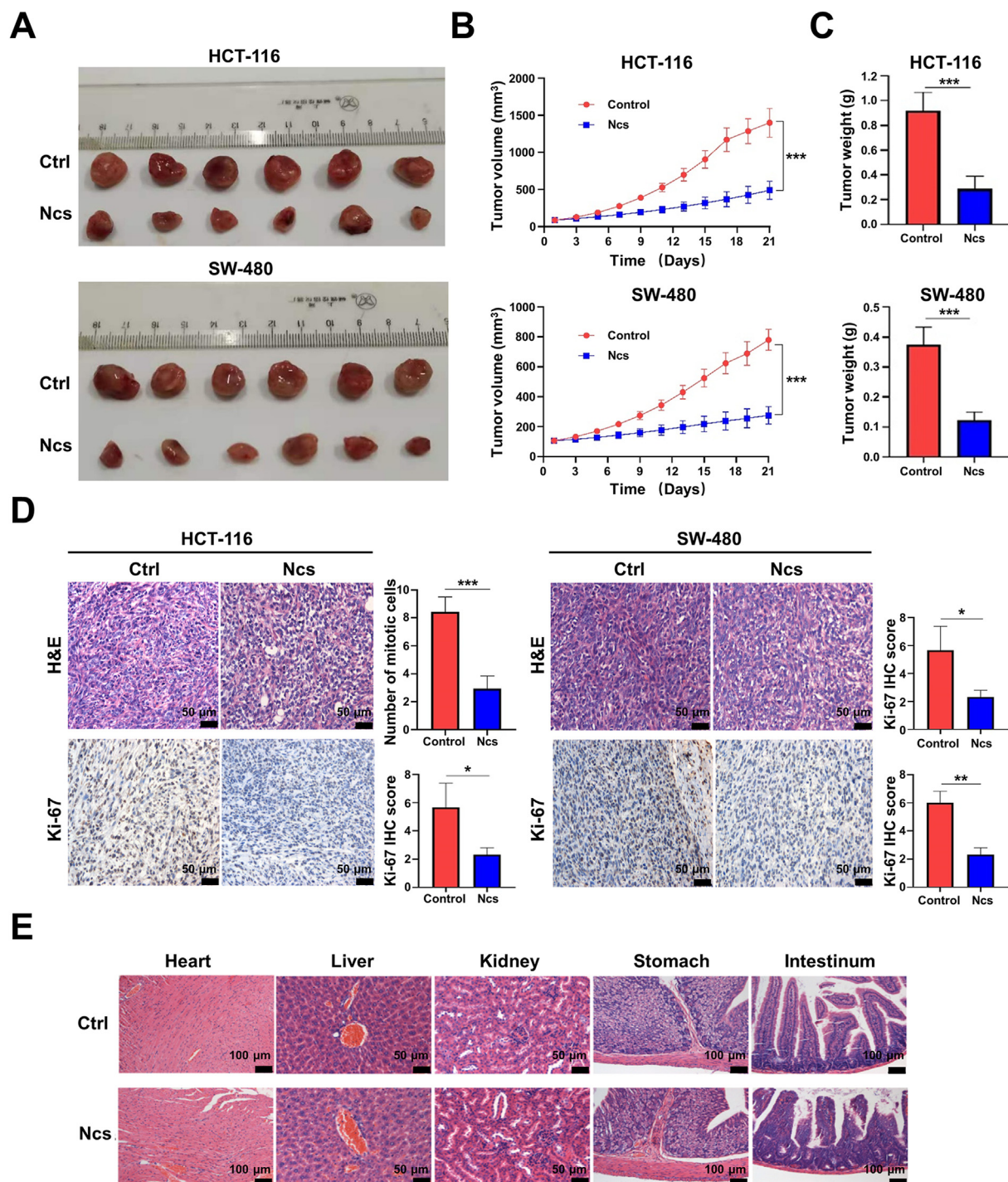
Figure 5 Ncs exhibits anti-colon carcinoma effects *in vivo*. Subcutaneous transplantation of CC HCT-116 and SW-480 cells into nude mice was used to establish a solid *in vivo* tumor model with Ncs treatment for 21 days ($n = 6$). **(A)** The representative image of isolated tumor from control or Ncs-treated nude mice. **(B)** The volumes of tumors were measured at different times. **(C)** Tumor weights of nude mice after sacrifice. **(D)** H&E staining was used to observe the nuclear division and pathological state of CC cells and Ki67 expression in tumor xenografts was examined by immunohistochemistry after being treated for 21 days with Ncs at 5 mg/kg/day. Scale bar = 50 μm. **(E)** H&E stain analyses of heart, liver, kidney, stomach, and intestinum in HCT-116 cell xenograft mice treated with vehicle or Ncs (5 mg/kg/day). Scale bar = 50 or 100 μm. Data are given as the mean ± SD and are representative of 3 independent experiments. Statistical difference was assessed using a *t*-test.
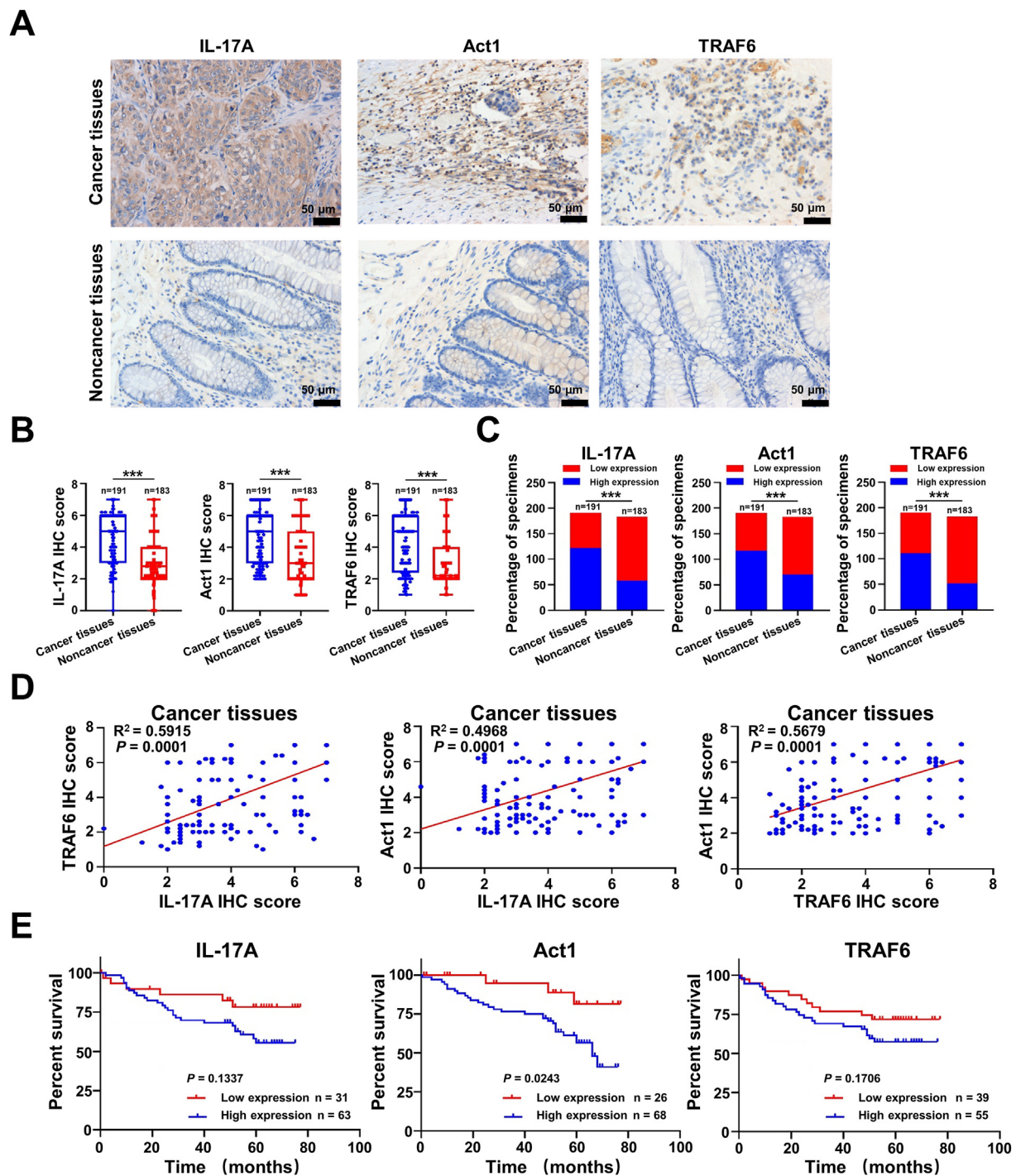
Figure 6 IL-17 A, Act1, and TRAF6 expression were up-regulated in CC tissue and were significantly correlated with poor prognosis. **(A)** Representative immunohistochemistry staining of IL-17 A, Act1, TRAF6 expression in CC tissue and non-cancer tissues. Scale bar = 50 μm. **(B)** Statistical analysis of immunohistochemical scores of IL-17 A, Act1, and TRAF6 in CC tissue and non-cancer tissues. **(C)** Percentage of high expression and low expression of IL-17 A, Act1, and TRAF6 in CC tissue and non-cancer tissues. **(D)** Pearson correlative analysis of staining scores for IL-17 A and Act1, L-17 A and TRAF6, as well as Act1 and TRAF6 in the CC tissue. **(E)** Overall survival durations of CC patients after Kaplan−Meier analysis were defined as low or high IL-17 A, Act1, or TRAF6 expression groups. Data are given as mean ± SD.

be up-regulated and acts to promote the proliferation of CC cells,[35] findings in good agreement with the present results. IL-17 A and TRAF6 expression were associated with poor tumor differentiation, as well as for Act1 expression with lymph node metastasis, in human CC specimens. These results suggest that the IL-17A/Act1/TRAF6 signaling axis is

Table 1 Correlation analyses of IL-17 A, Act1 and TRAF6 expression in colorectal cancer with clinicopathologic features.

Characteristics	No. of patients	IL-17 A		P	Act1		P	TRAF6		P
		High expression n (%)	Low expression n (%)		High expression n (%)	Low expression n (%)		High expression n (%)	Low expression n (%)	
Overall	191	120 (63.9%)	71 (36.1%)		117 (61.3%)	74 (38.7%)		111 (58.1%)	80 (41.9%)	
Age				0.99			0.51			0.48
<60 years, n (%)	70 (36.6%)	44 (62.8%)	26 (37.1%)		45 (64.2%)	25 (35.8%)		43 (61.4%)	27 (38.6%)	
≥60 years, n (%)	121 (63.4%)	76 (62.8%)	45 (37.1%)		72 (59.5%)	49 (40.5%)		68 (56.2%)	53 (43.8%)	
Gender				0.16			0.57			0.40
Female, n (%)	103 (53.9%)	60 (58.3%)	43 (41.7%)		65 (63.1%)	38 (36.9%)		57 (55.3%)	46 (44.7%)	
Male, n (%)	88 (46.1%)	60 (68.2%)	28 (31.8%)		52 (59.0%)	36 (41.0%)		54 (61.4%)	43 (38.6%)	
Tumor size				0.22			0.28			0.05
<5.0 cm, n (%)	94 (49.2%)	55 (58.5%)	39 (41.5%)		54 (57.4%)	40 (42.6%)		48 (51.1%)	46 (48.9%)	
≥5.0 cm, n (%)	97 (50.8%)	65 (67.0%)	32 (33.0%)		63 (64.9%)	34 (35.1%)		63 (64.9%)	34 (35.1%)	
TNM Stage				0.67			0.93			0.90
I + II, n (%)	106 (55.5%)	68 (64.1%)	38 (35.9%)		65 (61.3%)	41 (38.7%)		62 (58.5%)	44 (41.5%)	
III + IV, n (%)	85 (45.5%)	52 (61.2%)	33 (38.8%)		52 (61.2%)	33 (38.8%)		49 (57.6%)	36 (42.4%)	
Pathological type				0.16			0.96			0.50
Ulceration, n (%)	114 (59.7%)	67 (58.8%)	47 (41.2%)		70 (61.4%)	44 (38.6%)		64 (56.1%)	50 (43.9%)	
Elevated + infiltrating, n (%)	77 (40.3%)	53 (68.9%)	24 (31.1%)		47 (61.0%)	30 (39.0%)		47 (61.0%)	30 (39.0%)	
Differentiation				0.03			0.09			0.01
Well/Moderate, n (%)	145 (75.9%)	85 (58.6%)	60 (41.4%)		84 (57.9%)	61 (42.0%)		77 (53.1%)	68 (46.9%)	
Poor, n (%)	46 (24.1%)	35 (76.0%)	11 (34.0%)		33 (71.7%)	13 (28.2%)		34 (73.9%)	12 (26.8%)	
Lymph node metastases				0.22			0.002			0.84
Negative, n (%)	113 (59.2%)	75 (66.4%)	38 (33.6%)		59 (52.2%)	54 (47.8%)		65 (57.5%)	48 (42.5%)	
Positive, n (%)	78 (40.8%)	45 (57.7%)	33 (42.3%)		58 (74.3%)	20 (25.6%)		46 (59.0%)	32 (41.0%)	

Note: Statistical significance was determined using a χ^2-test.

Correlation between IL-17A expression and clinic characteristics

Univariable risk factor	OR (95%CI)	P-value
Age (< 60 VS. ≥ 60)	1.00 (0.54-1.82)	0.99
Gender (Male VS. Female)	0.65 (0.36-1.17)	0.16
Tumor size (< 5.0 cm VS. ≥ 5.0 cm)	0.69 (0.38-1.24)	0.22
TNM Stage (I + II VS. III + IV)	1.13 (0.62-2.04)	0.67
Pathological type (ulceration VS. elevated + infiltrating)	0.65 (0.35-1.18)	0.16
Differentiation (Well/Moderate VS. Poor)	0.44 (0.20-0.92)	**0.03**
Lymph node metastases (Negative VS. ≥ Positive)	1.44 (0.79-2.64)	0.22

Correlation between Act1 expression and clinic characteristics

Univariable risk factor	OR (95%CI)	P-value
Age (< 60 VS. ≥ 60)	1.23 (0.66-2.23)	0.51
Gender (Male VS. Female)	1.18 (0.66-2.11)	0.57
Tumor size (< 5.0 cm VS. ≥ 5.0 cm)	0.72 (0.40-1.29)	0.28
TNM Stage (I + II VS. III + IV)	1.00 (0.59-1.78)	0.93
Pathological type (ulceration VS. elevated + infiltrating)	1.01 (0.55-1.83)	0.96
Differentiation (Well/Moderate VS. Poor)	0.54 (0.27-1.08)	0.09
Lymph node metastases (Negative VS. ≥ Positive)	0.37 (0.20-0.70)	**0.002**

Correlation between TRAF6 expression and clinic characteristics

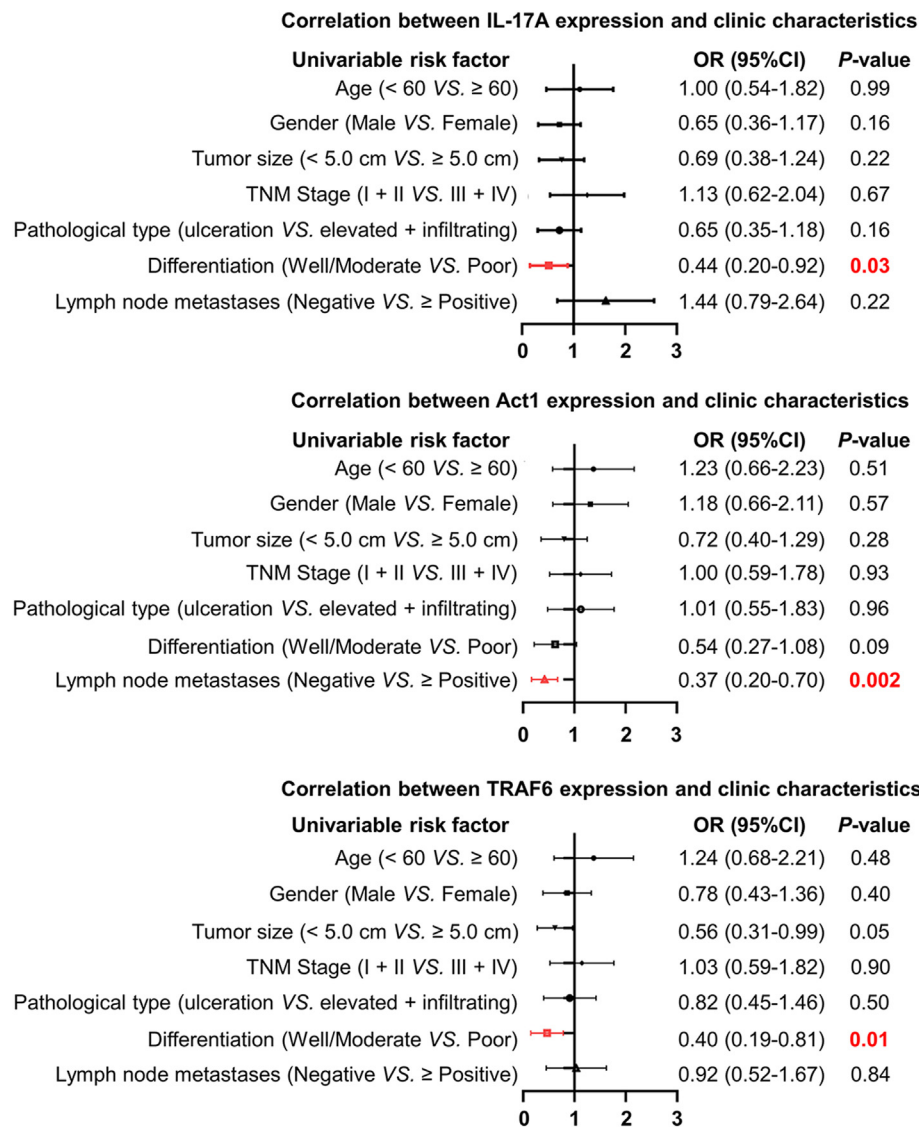| Univariable risk factor	OR (95%CI)	P-value
Age (< 60 VS. ≥ 60)	1.24 (0.68-2.21)	0.48
Gender (Male VS. Female)	0.78 (0.43-1.36)	0.40
Tumor size (< 5.0 cm VS. ≥ 5.0 cm)	0.56 (0.31-0.99)	0.05
TNM Stage (I + II VS. III + IV)	1.03 (0.59-1.82)	0.90
Pathological type (ulceration VS. elevated + infiltrating)	0.82 (0.45-1.46)	0.50
Differentiation (Well/Moderate VS. Poor)	0.40 (0.19-0.81)	**0.01**
Lymph node metastases (Negative VS. ≥ Positive)	0.92 (0.52-1.67)	0.84

Figure 7 Correlation of the expression of IL-17 A, Act1, and TRAF6 in CC with clinicopathologic features. The correlation between IL-17 A, Act1, and TRAF6 expression and CC patients' clinicopathologic characteristics in IHC analysis. There were obvious relationships between IL-17 A, TRAF6 expression and differentiation, the expression of Act1 and lymph node metastases. Statistical significance was determined using the χ^2-test.

involved in the genesis of CC and its continued development and that it can be used as a biomarker for the prognosis of CC patients and as a potential therapeutic target. Ncs can inhibit the IL-17A/Act1/TRAF6 signaling pathway, which is a potentially efficacious candidate for CC chemotherapy.

Conclusions

The results of *in vitro* and xenograft *in vivo* experiments revealed that Ncs blocked HCT-116 and SW-480 CC cell proliferation. Furthermore, mitochondrial apoptosis induction by inhibition of the anti-apoptotic IL-17A/Act1/TRAF6/NF-κB signaling pathway was demonstrated to underlie the mechanism of action of Ncs, which was partly reversed by IL-17 A substitution and enhanced by IL-17 A

silencing. Moreover, IL-17 A, Act1, and TRAF6 exhibited enhanced expression in CC tissue compared to noncancerous tissue, a finding associated with poor patient prognosis. It really should be regarded as a novel target for CC therapy.

Conflict of interests

The authors report no conflict of interests in this work.

Funding

Appendix A. Supplementary data

Supplementary data to this article can be found online at https://doi.org/10.1016/j.gendis.2023.03.014.

References

1. Xi Y, Xu P. Global colorectal cancer burden in 2020 and projections to 2040. *Transl Oncol*. 2021;14(10):101174.
2. Chung AS, Wu X, Zhuang G, et al. An interleukin-17-mediated paracrine network promotes tumor resistance to anti-angiogenic therapy. *Nat Med*. 2013;19(9):1114—1123.
3. Liu C, Liu R, Wang B, et al. Blocking IL-17A enhances tumor response to anti-PD-1 immunotherapy in microsatellite stable colorectal cancer. *J Immunother Cancer*. 2021;9(1), e001895.
4. Fabre J, Giustiniani J, Garbar C, et al. Targeting the tumor microenvironment: the protumor effects of IL-17 related to cancer type. *Int J Mol Sci*. 2016;17(9):1433.
5. Gaffen SL. Structure and signalling in the IL-17 receptor family. *Nat Rev Immunol*. 2009;9(8):556—567.
6. Shalom-Barak T, Quach J, Lotz M. Interleukin-17-induced gene expression in articular chondrocytes is associated with activation of mitogen-activated protein kinases and NF-κB. *J Biol Chem*. 1998;273(42):27467—27473.
7. Lereclus E, Tout M, Girault A, et al. A possible association of baseline serum IL-17A concentrations with progression-free survival of metastatic colorectal cancer patients treated with a bevacizumab-based regimen. *BMC Cancer*. 2017;17:220.
8. Wang D, Yuan W, Wang Y, et al. Serum CCL20 combined with IL-17A as early diagnostic and prognostic biomarkers for human colorectal cancer. *J Transl Med*. 2019;17:253.
9. Ren H, Wang Z, Zhang S, et al. IL-17A promotes the migration and invasiveness of colorectal cancer cells through NF-κB-mediated MMP expression. *Oncol Res*. 2016;23(5):249—256.
10. Kornienko A, Evidente A. Chemistry, biology, and medicinal potential of narciclasine and its congeners. *Chem Rev*. 2008; 108(6):1982—2014.
11. Fürst R. Narciclasine - an Amaryllidaceae alkaloid with potent antitumor and anti-inflammatory properties. *Planta Med*. 2016;82(16):1389—1394.
12. Cao H, Huang W, Zhang N, et al. Narciclasine induces autophagy-dependent apoptosis in triple-negative breast cancer cells by regulating the AMPK-ULK1 axis. *Cell Prolif*. 2018;51(6), e12518.
13. Van Goietsenoven G, Mathieu V, Lefranc F, et al. Narciclasine as well as other Amaryllidaceae isocarbostyrils are promising GTP-ase targeting agents against brain cancers. *Med Res Rev*. 2013;33(2):439—455.
14. Bräutigam J, Bischoff I, Schürmann C, et al. Narciclasine inhibits angiogenic processes by activation of Rho kinase and by downregulation of the VEGF receptor 2. *J Mol Cell Cardiol*. 2019;135:97—108.
15. Dumont P, Ingrassia L, Rouzeau S, et al. The Amaryllidaceae isocarbostyril narciclasine induces apoptosis by activation of the death receptor and/or mitochondrial pathways in cancer cells but not in normal fibroblasts. *Neoplasia*. 2007;9(9):766—776.
16. Deng H, Huang L, Liao Z, et al. Itraconazole inhibits the Hedgehog signaling pathway thereby inducing autophagy-mediated apoptosis of colon cancer cells. *Cell Death Dis*. 2020; 11(7):539.
17. Vidal S, Puig L, Carrascosa-Carrillo JM, et al. From messengers to receptors in psoriasis: the role of IL-17RA in disease and treatment. *Int J Mol Sci*. 2021;22(13):6740.
18. Wu D, Wu P, Huang Q, et al. Interleukin-17: a promoter in colorectal cancer progression. *Clin Dev Immunol*. 2013;2013: 436307.
19. Kryczek I, Wu K, Zhao E, et al. IL-17+ regulatory T cells in the microenvironments of chronic inflammation and cancer. *J Immunol*. 2011;186(7):4388—4395.
20. Yang S, Wang B, Guan C, et al. Foxp3+ IL-17+ T cells promote development of cancer-initiating cells in colorectal cancer. *J Leukoc Biol*. 2011;89(1):85—91.
21. Hyun YS, Han DS, Lee AR, et al. Role of IL-17A in the development of colitis-associated cancer. *Carcinogenesis*. 2012; 33(4):931—936.
22. Housseau F, Wu S, Wick EC, et al. Redundant innate and adaptive sources of IL17 production drive colon tumorigenesis. *Cancer Res*. 2016;76(8):2115—2124.
23. Ali ET, Masri MAM, Siddig EE, et al. Immunohistochemical expression of interleukin-17 and hormonal receptors in benign and malignant breast lesions. *BMC Res Notes*. 2020;13: 300.
24. Chang YH, Yu CW, Lai LC, et al. Up-regulation of interleukin-17 expression by human papillomavirus type 16 E6 in nonsmall cell lung cancer. *Cancer*. 2010;116(20):4800—4809.
25. Cao HX, Zhang W, Liang J. Inhibition of IL17A promotes bufalin-induced apoptosis in colon cancer cells via miR-96/DDIT3. *Int J Clin Exp Pathol*. 2016;9:4360—4367.
26. Steiner GE, Newman ME, Paikl D, et al. Expression and function of pro-inflammatory interleukin IL-17 and IL-17 receptor in normal, benign hyperplastic, and malignant prostate. *Prostate*. 2003;56(3):171—182.
27. Do Thi VA, Park SM, Lee H, et al. The membrane-bound form of IL-17A promotes the growth and tumorigenicity of colon cancer cells. *Mol Cell*. 2016;39(7):536—542.
28. Hu C, Zhang X, Wei W, et al. Matrine attenuates oxidative stress and cardiomyocyte apoptosis in doxorubicin-induced cardiotoxicity *via* maintaining AMPKα/UCP₂ pathway. *Acta Pharm Sin B*. 2019;9(4):690—701.
29. Wang X. The expanding role of mitochondria in apoptosis. *Genes Dev*. 2001;15(22):2922—2933.
30. Green DR, Reed JC. Mitochondria and apoptosis. *Science*. 1998; 281(5381):1309—1312.
31. Martinou JC, Youle RJ. Mitochondria in apoptosis: Bcl-2 family members and mitochondrial dynamics. *Dev Cell*. 2011;21(1): 92—101.
32. Asakura T, Ohkawa K. Chemotherapeutic agents that induce mitochondrial apoptosis. *Curr Cancer Drug Targets*. 2004;4(7): 577—590.
33. Soleimani A, Rahmani F, Ferns GA, et al. Role of the NF-κB signaling pathway in the pathogenesis of colorectal cancer. *Gene*. 2020;726:144132.
34. Cui G, Yuan A, Goll R, et al. IL-17A in the tumor microenvironment of the human colorectal adenoma—carcinoma sequence. *Scand J Gastroenterol*. 2012;47(11):1304—1312.
35. Sun H, Li X, Fan L, et al. TRAF₆ is upregulated in colon cancer and promotes proliferation of colon cancer cells. *Int J Biochem Cell Biol*. 2014;53:195—201.